

## Wave chaos in quantum billiards with a small but finite-size scatterer

T. Shigehara

*Computer Centre, University of Tokyo, Yayoi, Bunkyo-ku, Tokyo 113, Japan*

Taksu Cheon

*Department of Physics, Hosei University, Fujimi, Chiyoda-ku, Tokyo 102, Japan*

(Received 17 January 1996)

We study the low-energy quantum spectra of two-dimensional rectangular billiards with a small but finite-size scatterer inside. We start by examining the spectral properties of billiards with a single pointlike scatterer. The problem is formulated in terms of the self-adjoint extension theory of functional analysis. The condition for the appearance of so-called wave chaos is clarified. We then relate the pointlike scatterer to a finite-size scatterer through an appropriate truncation of the basis. We show that the signature of wave chaos in low-energy states is most prominent when the scatterer is weakly attractive. As an illustration, numerical results of a rectangular billiard with a small rectangular scatterer inside are exhibited. [S1063-651X(96)08908-8]

PACS number(s): 05.45.+b, 03.65.Db

### I. INTRODUCTION

The two-dimensional billiard is an appropriate tool for examining generic features of dynamical systems because of the wide range of dynamical behaviors, going from the most regular (integrable) to the most irregular (chaotic) depending on the geometry of its boundary. Although no mathematical proof exists, it is widely believed that fingerprints of the regular or irregular nature of the classical motion can be found in statistical properties of the quantum spectrum both in energy levels and wave functions. Integrable systems such as circular, elliptic, and rectangular billiards obey Poisson statistics [1,2], while the predictions of the Gaussian orthogonal ensembles describe chaotic systems such as Sinai's billiard and Bunimovich's stadium [3,4].

Besides these extreme classes, there is an intermediate category called a *pseudointegrable* [5,6] or *almost integrable* [7] system. Typical examples are staircase billiards [8], rational polygons [5,9–11], and billiards with pointlike scatterers inside an integrable one [12–17]. The nature of classical motion in pseudointegrable systems can be considered as integrable in the sense that unstable trajectories are of measure zero. However, several numerical studies have revealed that, under a certain condition, quantization induces the chaotic energy spectra, which can be regarded as a counterexample for the correspondence between the energy spectra and the underlying classical motion. This phenomenon is called *wave chaos* because its origin is the wavelike nature of quantum motion. For billiards with pointlike scatterers, this phenomenon has been understood in terms of the quantum breaking of the classical scale invariance [17]. However, the notion of the pointlike scatterer is a mathematical abstraction whose relevance to the physical system is far from straightforward. It is therefore highly desirable to show that the nature of wave chaos remains intact for the case of a finite-size scatterer. This is the prime motivation of the work we report in this paper. We restrict ourselves to considering billiards with a small but finite-size scatterer inside an integrable one. It is shown that, even if the scatterer has a substantial size, the signature of wave chaos is observable under a certain

condition. The condition is consistent with a previous numerical observation in Sinai's billiard, which indicates that there exists no signature of wave chaos when the scatterer is repulsive.

The paper is organized as follows. We start by examining the spectral properties of pseudointegrable billiards with a pointlike scatterer in Secs. II and III. In the former section, we give an accurate description of a pointlike scatterer, based on the self-adjoint extension theory in functional analysis. A special emphasis is laid on the distinction between symmetry and self-adjointness. We give an intuitive explanation of the necessity of the self-adjointness for quantum mechanical Hamiltonians. Applying a general prescription for extending a symmetric operator to a self-adjoint one, we derive the Green's function for billiards with a single pointlike scatterer. A renormalized coupling constant of the scatterer is defined in a natural manner, although its physical meaning is somewhat unclear at this stage. Based on the formulation in Sec. II, we discuss the quantum spectra of billiards with a pointlike scatterer in Sec. III. The general condition for the appearance of wave chaos is clarified. In Sec. IV, we consider a Dirac's  $\delta$  function potential with a truncated basis. Although it is not well defined with a full basis in two-dimensional billiards, we can deduce certain physical contents from the truncated system, which serve as the basis for the ensuing discussions. The findings in Secs. III and IV are applied to the cases of a small but finite-size scatterer in Sec. V. It is shown that the wave chaos is manifest at low energy with attractive potentials. As an illustration, we give a numerical example of a rectangular billiard with a small rectangular scatterer inside. We also show a proper procedure for the zero-size limit of the finite-size scatterer, which is consistent with the self-adjointness of the Hamiltonian. This clarifies the physical meaning of the renormalized coupling constant defined in Sec. II. We give conclusions in Sec. VI.

### II. QUANTUM MECHANICAL FORMULATION OF PSEUDOINTEGRABLE BILLIARDS WITH A POINTLIKE SCATTERER

In spite of the apparent simplicity, careful treatments are required for a definition of quantum billiards with a pointlike

scatterer inside. Several methods are known for this purpose [18]. Here we adopt one based on the self-adjoint extension theory in functional analysis [19]. We briefly summarize the formalism, stressing the necessary points for discussions in following sections. We also mention the physical reasons why quantum mechanics requires self-adjointness for Hamiltonians.

Let us consider an integrable billiard of area  $S$  with the Dirichlet boundary condition such that wave functions vanish on the boundary. The eigenvalues and corresponding eigenfunctions are determined by the stationary Schrödinger equation

$$H_0 \varphi_n(\vec{x}) \equiv -\frac{1}{2M} \Delta \varphi_n(\vec{x}) = E_n \varphi_n(\vec{x}) \quad (n = 1, 2, 3, \dots), \tag{1}$$

where  $\vec{x}$  is the coordinate vector in two-dimensional space, and  $M$  is the mass of a particle moving in the billiard. We adopt natural units throughout this paper:  $\hbar = 1$  and  $c = 1$ . This leaves a single independent unit among mass, energy, and length. The domain of  $H_0$  is  $D(H_0) = H^2(S) \cap H_0^1(S)$  in terms of the Sobolev spaces. (We denote the domain of the billiard by the same symbol as the area unless there is danger of confusion.) In the following, we assume that the unperturbed billiard has no degeneracy. The Green's function of this system is given by

$$G^{(0)}(\vec{x}, \vec{y}; z) = \sum_{n=1}^{\infty} \frac{\varphi_n(\vec{x}) \varphi_n(\vec{y})}{z - E_n}, \tag{2}$$

where  $z$  is an energy variable. Suppose that a pointlike scatterer is placed at  $\vec{x} = \vec{x}_0$  inside the billiard. Following the self-adjoint extension theory in functional analysis, the eigenvalues and corresponding eigenfunctions of the perturbed system are calculated as follows.

The first step for this purpose is to remove the relevant scattering point  $\vec{x}_0$  by restricting  $H_0$  to  $T = H_0|D(T)$  with the domain

$$D(T) = \{\varphi(\vec{x}) \in D(H_0) | \varphi(\vec{x}_0) = 0\}. \tag{3}$$

By using integration by parts, it is easy to see that  $T$  is symmetric (Hermitian). However, the domain of  $T^*$ , the adjoint operator of  $T$ , is not identical to  $D(T)$ , and is indeed larger than  $D(T)$ :

$$D(T^*) = D(T) \oplus R(T - \bar{\lambda})^\perp \oplus R(T - \lambda)^\perp, \tag{4}$$

where  $R(T - \lambda)^\perp$ , which is the orthogonal complement to the range of  $T - \lambda$ , corresponds to the deficiency subspace of  $T$  given by [20]

$$R(T - \lambda)^\perp = \{\varphi(\vec{x}) | \varphi(\vec{x}) = c G^{(0)}(\vec{x}, \vec{x}_0; \bar{\lambda}), c \in \mathbf{C}\}, \tag{5}$$

with an arbitrary complex number  $\lambda$  ( $\text{Im} \lambda \neq 0$ ). It follows from  $D(T^*) \neq D(T)$  that  $T$  is not self-adjoint. A symmetric operator is self-adjoint if and only if  $D(T^*) = D(T)$ .

The two following facts serve to understand the reason for imposing self-adjointness on quantum mechanical Hamiltonians [21,22]. One of them is based on the assertion

$$N(T^* - \bar{\lambda}) = R(T - \lambda)^\perp \quad (\text{Im} \lambda \neq 0), \tag{6}$$

where  $N(A)$  is the null space (or kernel) of the operator  $A$ . This means that  $T^*$  has a complex eigenvalue  $\bar{\lambda}$  with eigenspace  $R(T - \lambda)^\perp$ . If and only if  $T$  is self-adjoint,  $R(T - \lambda)^\perp = \emptyset$ , i.e.,  $R(T - \lambda)$  is the entire Hilbert space  $X = L^2(S)$ , the set of all square-integrable functions over  $S$ . This is one of the reasons why quantum mechanics, which does not allow complex eigenvalues for observables, requires self-adjoint Hamiltonians. The second fact is closely related to the unitarity of time-evolution operators. The time-evolution operator  $U(t)$  is constructed from  $T$  as follows;

$$U(t) \equiv e^{-iTt} = \lim_{n \rightarrow \infty} \left( 1 + \frac{iTt}{n} \right)^{-n} = \lim_{n \rightarrow \infty} \left\{ \left( \frac{it}{n} \right)^{-n} \left( T - \frac{in}{t} \right)^{-n} \right\}. \tag{7}$$

It is easy to see that, for any symmetric  $T$ , an operator  $(T - \lambda)^{-1}$  with pure imaginary  $\lambda \neq 0$  is defined from  $R(T - \lambda)$  to  $D(T)$  with  $\|(T - \lambda)^{-1} \varphi\| \leq \|\varphi\| / |\text{Im} \lambda|$  for any  $\varphi \in R(T - \lambda)$ . If  $R(T - \lambda)$  is not all of  $X$ , then, in general,  $(T - \lambda)^{-n}$  can be defined on smaller and smaller spaces as  $n$  increases. This leads us to a natural condition  $R(T - \lambda) = X$ , implying that time-evolution operators which preserve probability can be constructed only from self-adjoint operators.

The above considerations indicate that we have to extend  $D(T)$ , or equivalently, restrict  $D(T^*)$ , in order to construct a self-adjoint operator from  $T = H_0|D(T)$ . This is indeed possible since  $\dim R(T - \bar{\lambda})^\perp = \dim R(T - \lambda)^\perp$ . Because both the deficiency subspaces are one-dimensional, a one-parameter family of self-adjoint extensions of  $T$  exist. According to a general prescription for extending a symmetric operator to self-adjoint ones [23], all the self-adjoint extensions of  $T$  are given by  $H_\theta = H_0$  ( $0 \leq \theta < 2\pi$ ) with the domain

$$D(H_\theta) = \{\psi(\vec{x}) | \psi(\vec{x}) = \varphi(\vec{x}) + c G^{(0)}(\vec{x}, \vec{x}_0; \lambda) - c e^{i\theta} G^{(0)}(\vec{x}, \vec{x}_0; \bar{\lambda});$$

$$\varphi(\vec{x}) \in D(T),$$

$$G^{(0)}(\vec{x}, \vec{x}_0; \lambda) \in R(T - \bar{\lambda})^\perp,$$

$$G^{(0)}(\vec{x}, \vec{x}_0; \bar{\lambda}) \in R(T - \lambda)^\perp, c \in \mathbf{C}\}. \tag{8}$$

Equation (6) with Eq. (5) indicates that the operation of  $H_\theta$  on  $\psi(\vec{x})$  is given by

$$(H_\theta \psi)(\vec{x}) = (H_0 \varphi)(\vec{x}) + \lambda c G^{(0)}(\vec{x}, \vec{x}_0; \lambda) - \bar{\lambda} c e^{i\theta} G^{(0)}(\vec{x}, \vec{x}_0; \bar{\lambda}). \tag{9}$$

The operator  $H_\theta$  is regarded as the Hamiltonian of the perturbed system with a pointlike scatterer. Notice that, al-

though we have  $H_\theta = H_0$  on  $D(T)$ ,  $D(H_\theta)$  is substantially larger than  $D(T)$ :  $D(T) \subset D(H_\theta) \subset D(T^*)$ . We recognize from the second and third terms of  $\psi(\vec{x})$  in Eq. (8) that the appropriate boundary condition around the scatterer is specified after the extension. It will be shown below that the value of  $\theta$  is related to the strength of the pointlike scatterer.

With the aid of the resolvent equation, we can write an

equation for the Green's function of the system with the Hamiltonian  $H_\theta$  as

$$G_\theta(\vec{x}, \vec{y}; z) = G^{(0)}(\vec{x}, \vec{y}; z) + G^{(0)}(\vec{x}, \vec{x}_0; z) T_\theta(z) G^{(0)}(\vec{x}_0, \vec{y}; z), \quad (10)$$

where the transition matrix ( $T$  matrix)  $T_\theta(z)$  is calculated through

$$T_\theta(z) = \frac{1 - e^{i\theta}}{(z - \lambda) \int_S G^{(0)}(\vec{x}, \vec{x}_0; z) G^{(0)}(\vec{x}, \vec{x}_0; \lambda) d\vec{x} - e^{i\theta} (z - \bar{\lambda}) \int_S G^{(0)}(\vec{x}, \vec{x}_0; z) G^{(0)}(\vec{x}, \vec{x}_0; \bar{\lambda}) d\vec{x}}. \quad (11)$$

After substituting Eq. (2) into Eq. (11), and with a somewhat lengthy but straightforward calculation, we have

$$T_\theta(z) = [v_\theta^{-1} - G(z)]^{-1}, \quad (12)$$

where

$$v_\theta^{-1} = |\lambda| \frac{\sin\left(\frac{\theta}{2} + \arg\lambda\right)}{\sin\frac{\theta}{2}} \sum_{n=1}^{\infty} \frac{\varphi_n(\vec{x}_0)^2}{|E_n - \lambda|^2}, \quad (13)$$

$$G(z) = \sum_{n=1}^{\infty} \varphi_n(\vec{x}_0)^2 \left( \frac{1}{z - E_n} + \frac{E_n}{|E_n - \lambda|^2} \right). \quad (14)$$

It follows from Eq. (12) that the perturbed eigenvalues are determined by

$$G(z) = v_\theta^{-1}. \quad (15)$$

The solutions of this equation  $z_n$  ( $n = 1, 2, 3, \dots$ ) correspond to the poles of the  $T$  matrix. The corresponding eigenfunction is the residue of the Green's function of Eq. (10) at the pole,

$$\psi_n(\vec{x}) = N_n G^{(0)}(\vec{x}, \vec{x}_0; z_n), \quad (16)$$

where the normalization factor is determined by

$$N_n^{-2} = \sum_{k=1}^{\infty} \frac{\varphi_k(\vec{x}_0)^2}{(z_n - E_k)^2}. \quad (17)$$

Although the  $T$  matrix seemingly has two independent parameters  $\lambda$  and  $\theta$ , this is not the case. This follows from the fact that  $|\lambda|$  is regarded as a scale of mass in case of  $\lambda$  being pure imaginary. Indeed, taking  $|\lambda|$  as a unit of energy, we can fix  $\lambda = +i$ , which makes all the relevant physical quantities dimensionless. Such a treatment is justified by the

assertion that a symmetric operator  $T$  is self-adjoint if the condition  $R(T - \lambda) = R(T - \bar{\lambda}) = X$  is valid for *some fixed*  $\lambda$  ( $\text{Im}\lambda \neq 0$ ). This means that if and only if  $R(T \pm i) = X$ , a symmetric operator  $T$  is self-adjoint. Thus, without any loss of generality, we can make the replacement of  $|\lambda| \rightarrow 1$ ,  $z \rightarrow |\lambda|z$ ,  $E_n \rightarrow |\lambda|E_n$  and  $\varphi_n \rightarrow |\lambda|\varphi_n$  in Eqs. (13), (14), and (15). We then have

$$\bar{G}(z) = \bar{v}_\theta^{-1}, \quad (18)$$

where

$$\bar{v}_\theta^{-1} = \frac{\sin\theta}{1 - \cos\theta} \sum_{n=1}^{\infty} \frac{\varphi_n(\vec{x}_0)^2}{E_n^2 + 1}, \quad (19)$$

$$\bar{G}(z) = \sum_{n=1}^{\infty} \varphi_n(\vec{x}_0)^2 \left( \frac{1}{z - E_n} + \frac{E_n}{E_n^2 + 1} \right). \quad (20)$$

We can regard  $\bar{v}_\theta$  as a coupling constant of a pointlike scatterer. It ranges over all real numbers as  $0 \leq \theta < 2\pi$ .

In a previous publication [16], we referred to the coupling constant  $\bar{v}_\theta$  as the bare coupling constant, denoted by  $v_B$ . However, this is somewhat confusing, because  $\bar{v}_\theta$  should be considered to arise in a renormalization process for treating short-range singularities in a proper manner, which we often encounter in field theory. It might be more appropriate to call  $\bar{v}_\theta$  the *renormalized coupling constant*.

Because the average level density of two-dimensional billiards is independent of energy  $z$ , each term in the parentheses of Eq. (20) diverges when summed separately. The divergence disappears when summed together. This means that the second term of Eq. (20) plays an essential role to make the  $T$  matrix well defined. It is also noteworthy that the energy dependence appears only in the first term of Eq. (20). This ensures the orthogonality of the perturbed eigenfunctions  $\{\psi_n(\vec{x})\}$  ( $n = 1, 2, 3, \dots$ ). That is, for  $m \neq n$ , we have

$$\int_S \psi_m(\vec{x}) \psi_n(\vec{x}) d\vec{x} = N_m N_n \frac{\bar{G}(z_n) - \bar{G}(z_m)}{z_m - z_n} = 0. \quad (21)$$

The orthonormal relations of the unperturbed eigenfunctions  $\{\varphi_n(\vec{x})\}$  ( $n=1,2,3,\dots$ ) are used in the first equality, and the second equality results from Eq. (18). The authors of Ref. [24] have discussed a rectangular billiard with a single pointlike scatterer, and deduced an eigenvalue equation, Eq. (23) in Ref. [24], which is seemingly analogous to Eq. (18) with Eqs. (19) and (20) in this paper. However, there is one crucial difference between them. The authors of Ref. [24] started with the assumption that the transition matrix is energy independent, which does not agree with Eq. (12) in this paper, and, as a result, the divergence appeared in  $G^{(0)}(\vec{x},\vec{x}_0;z)$  in the vicinity of the scatterer,  $\vec{x}\approx\vec{x}_0$ , is regularized by a logarithmically energy-dependent term, while the coupling strength remains constant in Eq. (23) in Ref. [24]. This is nothing but the coupling strength  $\bar{v}_\theta$  changing according to the energy in Eq. (18) in this paper, leading to a violation of the orthogonality of the perturbed eigenfunctions as well as the unitarity of the time-evolution operator.

### III. QUANTUM SPECTRUM OF PSEUDOINTEGRABLE BILLIARDS WITH A POINTLIKE SCATTERER

Equipped with the formulation in Sec. II, we examine the spectral properties of pseudointegrable billiards with a pointlike scatterer. A special emphasis is placed on the condition for the appearance of wave chaos.

An important fact is that each perturbed eigenvalue is isolated between two unperturbed ones. This follows from the fact that  $\bar{G}(z)$  of Eq. (20) is a monotonically decreasing function of  $z$  on the interval between any two successive unperturbed eigenvalues,  $(E_n, E_{n+1})$ , covering the entire value between  $(-\infty, \infty)$ . It is also clear that  $\bar{G}(z)$  has a single inflection point on  $(E_n, E_{n+1})$ . We have shown in Ref. [16] that the disturbance by the pointlike scatterer is restricted to eigenstates with an eigenvalue around which  $\bar{G}(z)$  has an inflection point (see Figs. 2 and 3 in Ref. [16]). This is understood also from the eigenfunction Eq. (16) with Eq. (2); if a perturbed eigenvalue is close to an unperturbed one, the corresponding perturbed eigenfunction is not substantially different from the corresponding unperturbed one.

In Ref. [16], the condition for the inflection points has been deduced in a somewhat complicated manner, by making a truncation of the unperturbed basis according to the energy under consideration. Here we refine the argument without introducing any truncation of the basis.

Each inflection point of  $\bar{G}(z)$ , say  $\tilde{z}_m$  ( $m=1,2,3,\dots$ ), is expected to appear, on average, around the midpoint on  $(E_m, E_{m+1})$ ,  $\tilde{z}_m \approx (E_m + E_{m+1})/2$ . Since the average level density of the unperturbed system is  $\rho_{\text{av}} = MS/(2\pi)$  according to the Weyl's theorem, the unperturbed energies are distributed, on average, at regular intervals  $\rho_{\text{av}}^{-1}$ . Furthermore, the average of  $\varphi_n(\vec{x}_0)^2$  among various  $n$  is independent of the energy,  $\langle \varphi_n(\vec{x}_0)^2 \rangle \approx 1/S$  for a generic choice of  $\vec{x}_0$ . Thus the contributions from  $0 < E_n < \tilde{z}_m$  and  $\tilde{z}_m < E_n < 2\tilde{z}_m \approx E_{2m}$  on the summation of the first term in Eq. (20) are canceled with a high degree of accuracy. This allows us to estimate  $\bar{G}(z)$  at the inflection point  $\tilde{z}_m$  as follows:

$$\begin{aligned} \bar{G}(\tilde{z}_m) &\approx \sum_{n=1}^{2m} \varphi_n(\vec{x}_0)^2 \frac{E_n}{E_n^2 + 1} \\ &\quad + \sum_{n=2m+1}^{\infty} \varphi_n(\vec{x}_0)^2 \left( \frac{1}{\tilde{z}_m - E_n} + \frac{E_n}{E_n^2 + 1} \right) \\ &\approx \alpha \left\{ \int_0^{E_{2m}} \frac{E}{E^2 + 1} dE + \int_{E_{2m}}^{\infty} \left( \frac{1}{\tilde{z}_m - E} + \frac{E}{E^2 + 1} \right) dE \right\} \\ &\approx \alpha \ln \tilde{z}_m, \end{aligned} \quad (22)$$

where we define

$$\alpha = \rho_{\text{av}} \langle \varphi_n(\vec{x}_0)^2 \rangle \approx \frac{M}{2\pi}. \quad (23)$$

It follows from Eqs. (18) and (22) that the effects of the pointlike scatterer on the quantum spectrum are observed in the eigenstates with an eigenvalue  $z$  such that

$$\alpha \ln z \approx \bar{v}_\theta^{-1}. \quad (24)$$

The condition of Eq. (24) corresponds to Eq. (60) in Ref. [16]. It is also noteworthy that an  $s$ -wave phase shift of the two-dimensional scattering problem with a single pointlike scatterer shows a similar logarithmic dependence on energy  $z$  [18,25]. The origin of such an energy dependence is closely related to the energy scale  $|\lambda|$  introduced by the self-adjoint extension of a symmetric operator; any function which depends on  $|\lambda|$  has an energy dependence, so as to guarantee the argument to be dimensionless. Although the nature of a particle motion in billiards is independent of the energy in classical physics, the singularity of the interaction induces an energy dependence of the observables after quantization. This can be considered as a typical example of quantum mechanical breaking of scale invariance, or *scale anomaly* [17,25].

Let us proceed to make an estimate of the width of a strip along the logarithmic curve of Eq. (24) on which the disturbance of the scatterer is observable. Using the derivative of  $\bar{G}(z)$  at an inflection point  $\tilde{z}_m$ , we can estimate the width, say  $\Delta$ , as follows:

$$\Delta \ll |\bar{G}'(\tilde{z}_m)| \rho_{\text{av}}^{-1} \approx \langle \varphi_n(\vec{x}_0)^2 \rangle \sum_{n=1}^{\infty} \frac{2}{\{(n - \frac{1}{2})\rho_{\text{av}}^{-1}\}^2} \rho_{\text{av}}^{-1}. \quad (25)$$

We have implicitly assumed in Eq. (25) that the unperturbed eigenvalues are distributed within a mean interval  $\rho_{\text{av}}^{-1}$  in the whole energy region including negative energies. This assumption is quite satisfactory in this case, because the denominator of  $\bar{G}'(z)$  is of the order of  $(z - E_n)^2$ , indicating that the summation in Eq. (25) converges rapidly. With the aid of a relation

$$\sum_{n=1}^{\infty} \frac{1}{(2n-1)^2} = \frac{\pi^2}{8}, \quad (26)$$

we arrive at

$$|\bar{G}'(\tilde{z}_m)|_{\rho_{av}^{-1}} \approx \pi^2 \alpha, \quad (27)$$

which means

$$\Delta \approx \alpha. \quad (28)$$

The estimate of Eq. (28) is justified from another perspective later in this paper.

The above considerations lead us to the condition for the appearance of wave chaos. The effect of a pointlike scatterer with strength  $\bar{v}_\theta$  appears mainly in the eigenstates with an eigenvalue  $z$ , satisfying

$$|\bar{v}_\theta^{-1} - \alpha \ln z| \leq \Delta. \quad (29)$$

In other words, wave chaos occurs in the energy region which satisfies

$$\exp\left\{\frac{1}{\alpha\bar{v}_\theta} - 1\right\} \leq z \leq \exp\left\{\frac{1}{\alpha\bar{v}_\theta} + 1\right\}. \quad (30)$$

These conditions are corroborated by the numerical experiments of the spectral statistics of rectangular billiards with a pointlike scatterer (see Figs. 5 and 6 in Ref. [16]). The condition of Eq. (29) contains all the essential physics of wave chaos. From this, we can draw the following conclusions.

(1) For any positive  $\bar{v}_\theta$ , wave chaos appears at the energy which satisfies Eq. (29), while it is hardly seen in other energies. If  $\bar{v}_\theta$  is larger than  $\Delta^{-1}$ , wave chaos appears only around the ground state region. As the energy increases, it tends to disappear. On the other hand, if  $\bar{v}_\theta$  is substantially smaller than  $\Delta^{-1}$ , wave chaos appears in the higher-energy region specified by Eq. (30). In the limit of  $\bar{v}_\theta \rightarrow +0$ , the system restores the integrability by pushing up the chaotic region to the infinite energy. (In this limit, the eigenvalue of the single eigenstate with an eigenvalue smaller than  $E_1$  diverges to  $-\infty$ .)

(2) Wave chaos does not appear at any energy if  $\bar{v}_\theta$  is negative. In particular, the system converges to the unperturbed one as  $\bar{v}_\theta \rightarrow -0$ .

(3) For any  $\bar{v}_\theta$ , the system behaves as integrable in the high-energy limit, which agrees with our intuition that a pointlike scatterer has no effect on a particle motion in the classical limit. In other words, quantum billiards with a pointlike scatterer have the nature of *asymptotic freedom*, which has been first discovered in the non-Abelian gauge field theories.

#### IV. FORMAL DESCRIPTION OF A POINTLIKE SCATTERER IN TERMS OF A DIRAC'S DELTA FUNCTION

We have revealed various features of two-dimensional billiards with a single pointlike scatterer from a general perspective in Sec. III. From a practical point of view, however, we still need to identify the physical meaning of the coupling strength  $\bar{v}_\theta$ , which does not have a direct relation to physical

observables. As a first step for this purpose, we show in this section that  $\bar{v}_\theta$  can be related to the physical strength of a pointlike scatterer through a truncation of the unperturbed basis.

Let us consider a *formal* Hamiltonian with a Dirac's  $\delta$  function potential

$$H = H_0 + v \delta(\vec{x} - \vec{x}_0) \quad (31)$$

with a truncated unperturbed basis  $\{\varphi_n(\vec{x})\}$  ( $n = 1, 2, 3, \dots, N$ ). We can regard  $v$  as the physical coupling constant of the pointlike scatterer. Notice that a Hamiltonian like Eq. (31) cannot be defined in billiard problems with higher dimension than 1, because one cannot take the limit of  $N \rightarrow \infty$ . For a moment, however, we will go further along with fixed  $N$ , and return to this point later in this section.

The characteristic equation of  $H$  is given by

$$\det(z\mathbf{I} - \mathbf{H}_0 - \mathbf{V}) = 0, \quad (32)$$

where  $\mathbf{I}$  is an  $N$ -dimensional unit matrix. The matrix elements of  $\mathbf{H}_0$  and  $\mathbf{V}$  are given by

$$(\mathbf{H}_0)_{mn} = E_n \delta_{mn} \quad (33)$$

and

$$(\mathbf{V})_{mn} = v \varphi_m(\vec{x}_0) \varphi_n(\vec{x}_0), \quad (34)$$

with  $m, n = 1, 2, 3, \dots, N$ , respectively. Using the linearity of a determinant and noticing that any two column vectors of  $\mathbf{V}$  are linearly dependent, we obtain

$$\begin{aligned} \det(z\mathbf{I} - \mathbf{H}_0 - \mathbf{V}) &= \prod_{n=1}^N (z - E_n) \\ &\quad - v \sum_{n=1}^N \left\{ \varphi_n^2(\vec{x}_0) \prod_{m=1}^N{}' (z - E_m) \right\}, \end{aligned} \quad (35)$$

where  $\Pi'$  signifies that the term of  $m = n$  is removed from the product. By inserting Eq. (35) into Eq. (32), the characteristic equation can be rewritten as

$$\tilde{G}(z) = v^{-1}, \quad (36)$$

where

$$\tilde{G}(z) = \sum_{n=1}^N \frac{\varphi_n(\vec{x}_0)^2}{z - E_n}. \quad (37)$$

For any  $v$ , Eq. (36) has  $N$  nondegenerate solutions  $z_n$  ( $n = 1, 2, 3, \dots, N$ ), giving a complete set of eigenvalues of the Hamiltonian Eq. (31) with the truncated basis. The corresponding eigenfunction is given by

$$\psi_n(\vec{x}) = N_n \sum_{k=1}^N \frac{\varphi_k(\vec{x}) \varphi_k(\vec{x}_0)}{z_n - E_k}, \quad (38)$$

with the normalization factor determined by

$$N_n^{-2} = \sum_{k=1}^N \frac{\varphi_k(\vec{x}_0)^2}{(z_n - E_k)^2}. \quad (39)$$

The eigenfunction Eq. (38) has a form analogous to Eq. (16). For large  $N$ , the appropriate boundary condition around the scatterer is taken into account in a matrix diagonalization with a Dirac's  $\delta$  function potential.

In an analysis similar to that in Sec. III, we recognize that the inflection points of  $\tilde{G}(z)$  are located around  $\tilde{G}(z) \approx 0$  at energy  $z \approx E_N/2$ , implying the appearance of wave chaos under the condition of  $v^{-1} \approx 0$ . We also expect that it disappears if  $|v^{-1}| \geq \Delta$ . In the case of  $|v^{-1}| \approx \Delta$ , the average ratio between the diagonal matrix element of the  $\delta$  function potential and the mean level spacing is estimated as

$$\left| \frac{\langle (\mathbf{V})_{nn} \rangle}{\rho_{\text{av}}^{-1}} \right| = \frac{\alpha}{\Delta} \approx 1. \quad (40)$$

This explains why the logarithmic curve of Eq. (24) has a strip with width  $\Delta$ ; in the case of  $|v^{-1}| \geq \Delta$ , the physical strength  $v$  is too weak to cause mixing among a large number of unperturbed eigenstates. In this sense, we can regard  $|v^{-1}|$  as a measure of distance to the wave-chaotic curve. We stress that  $|v^{-1}| \approx 0$  corresponds to the condition for the appearance of wave chaos in the energy region around  $z \approx E_N/2$ . Both at lower and higher energies, the value of  $\tilde{G}(z)$  at the inflection points is substantially different from zero, since contributions to  $\tilde{G}(z)$  from terms with  $E_n < z$  and  $E_n > z$  do not cancel. This fact gives rise to an interesting physical result in Sec. V.

Equation (37) allows us to relate the physical strength  $v$  to the formal strength  $\bar{v}_\theta$  introduced in Sec. II. In a similar manner as in Eq. (22), for  $z < E_N$  we obtain

$$\begin{aligned} \bar{G}(z) &= \tilde{G}(z) + \sum_{n=1}^N \varphi_n(\vec{x}_0)^2 \frac{E_n}{E_n^2 + 1} \\ &\quad + \sum_{n=N+1}^{\infty} \varphi_n(\vec{x}_0)^2 \left( \frac{1}{z - E_n} + \frac{E_n}{E_n^2 + 1} \right) \\ &\approx \tilde{G}(z) + \alpha \left\{ \int_0^{E_N} \frac{E}{E^2 + 1} dE \right. \\ &\quad \left. + \int_{E_N}^{\infty} \left( \frac{1}{z - E} + \frac{E}{E^2 + 1} \right) dE \right\} \\ &\approx \tilde{G}(z) + \alpha \ln(E_N - z). \end{aligned} \quad (41)$$

From Eqs. (18), (36), and (41), we obtain the relation between both the coupling constants,

$$\bar{v}_\theta^{-1} \approx v^{-1} + \alpha \ln(E_N - z). \quad (42)$$

We note that the summation in Eq. (37) diverges as  $N$  increases for any  $z \neq E_n$ . This follows from the fact that  $\alpha$  defined in Eq. (23) is independent of energy  $z$ . This underscores the fact that Dirac's  $\delta$  function potential with a full unperturbed basis cannot be defined in two-dimensional billiard problems, contrary to the case in one dimension. In the

latter case, since  $\alpha \propto \rho_{\text{av}}(z) \propto z^{-1/2}$ , the right-hand side of Eq. (37) converges. In this case, one can relate  $v$  with  $\bar{v}_\theta$  through

$$v^{-1} = \bar{v}_\theta^{-1} - \sum_{n=1}^{\infty} \varphi_n(\vec{x}_0)^2 \frac{E_n}{E_n^2 + 1}, \quad (43)$$

to make the matrix diagonalization with strength  $v$  identical to the formulation with  $\bar{v}_\theta$  discussed in Sec. II. Thus it is possible to construct quantum mechanics of one-dimensional billiards with a pointlike scatterer directly in terms of a Dirac's  $\delta$  function without relying on a somewhat complicated mathematical framework based on functional analysis. We finally emphasize that although the Hamiltonian with a Dirac's  $\delta$  function potential, Eq. (31), loses its meaning in the limit of  $N \rightarrow \infty$  in two-dimensional billiards, Eq. (42) is still valid for any  $v, \bar{v}_\theta$  if  $z < E_N$  with an arbitrarily fixed  $N$ .

## V. QUANTUM SPECTRUM OF BILLIARDS WITH A SMALL BUT FINITE-SIZE SCATTERER

In this section, we discuss the quantum spectra of billiards with a small but finite-size scatterer. We are after the wave-chaotic spectra in systems with a realistic finite-size scatterer inside. For this purpose, we attempt to describe the finite-size scatterer in terms of a Dirac's  $\delta$  function potential with a suitably truncated basis. This also enables us to recognize the physical meaning of the formal coupling constant  $\bar{v}_\theta$ . Relying on the arguments in Secs. III and IV, we clarify the condition for the appearance of wave-chaotic spectra for billiards with a small scatterer.

Suppose that a finite-size scatterer of area  $\Omega$  is placed at  $\vec{x} = \vec{x}_0$  inside an integrable billiard of area  $S$ . We describe the interaction in terms of a potential with a constant strength on the domain of the scatterer,

$$V(\vec{x}) = \begin{cases} V, & \vec{x} \in \Omega \\ 0, & \vec{x} \in S - \Omega, \end{cases} \quad (44)$$

where we denote the domains of the scatterer and the outer billiard by the same symbols as the areas. The matrix elements of  $V(\vec{x})$  are given by

$$(\mathbf{V})_{mn} = V \int_{\Omega} \varphi_m(\vec{x}) \varphi_n(\vec{x}) d\vec{x} \quad (m, n = 1, 2, 3, \dots). \quad (45)$$

If the area of the scatterer is far smaller than that of the outer billiard, the scatterer is expected to behave as pointlike at low energy because waves with long wavelength cannot "see" the shape of the scatterer. More precisely, the matrix element  $(\mathbf{V})_{mn}$  with  $E_m, E_n \leq (2M\Omega)^{-1}$  is suitably approximated by  $V\Omega \varphi_m(\vec{x}_0) \varphi_n(\vec{x}_0)$ . Furthermore, the off-diagonal matrix elements with  $E_m \ll (2M\Omega)^{-1} \ll E_n$  are small, because of the mismatch in the wave numbers. These indicate that the energy spectrum of the billiards with a finite-size scatterer of area  $\Omega$  can be reproduced by the Hamiltonian Eq. (31) in terms of a Dirac's  $\delta$  function potential with strength

$$v(\Omega) = V\Omega, \quad (46)$$

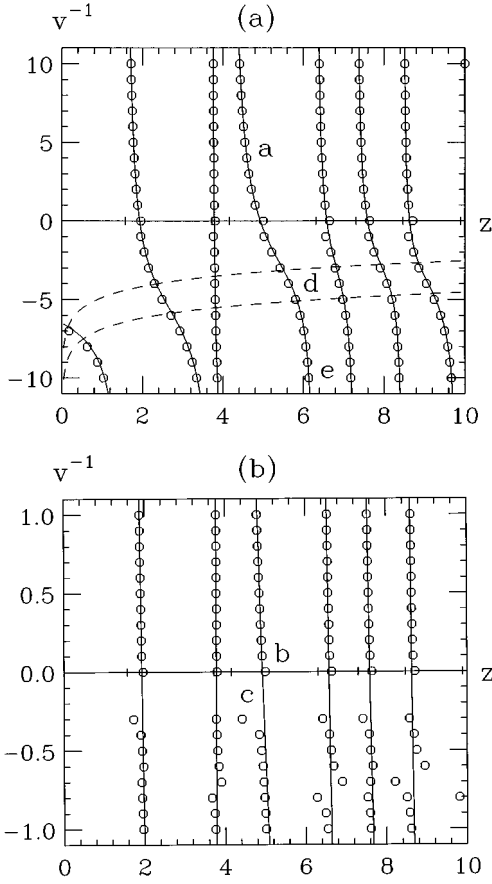


FIG. 1. Several lowest eigenvalues of a quantum particle of mass  $M=2\pi$  moving in the rectangular billiard of side lengths  $[l_x, l_y]=[1.047\ 19, 0.954\ 929]$  with a small rectangular scatterer inside. Side lengths and the location of the center of the inner scatterer are  $[\delta l_x, \delta l_y]=[3.538\ 30 \times 10^{-2}, 3.140\ 23 \times 10^{-2}]$  and  $\vec{x}_0=(0.622\ 482, 0.275\ 835)$ , respectively. In this choice, the area of the inner scatterer  $\Omega$  is  $1/900$ . The potential strength  $V$  is taken as constant on the inner scatterer. A circle located at  $(z, v^{-1})$  represents an eigenstate with eigenvalue  $z$  in case of potential strength  $V=v/\Omega=900/v^{-1}$ . The value of  $v^{-1}$  ranges from  $-10$  to  $10$  at intervals of  $1$  in (a), while it ranges from  $-1$  to  $-0.3$  and from  $0$  to  $1$  at intervals of  $0.1$  in (b). The case of  $v^{-1}=0$  is calculated by taking  $v=1000$  ( $V=900\ 000$ ). The solid curves are the approximated eigenvalues obtained by using the zero-range potential  $V(\vec{x})=v\delta(\vec{x}-\vec{x}_0)$ . These curves correspond to  $\tilde{G}(z)$  in Eq. (37). The unperturbed basis is truncated at  $E_{N(\delta l_x, \delta l_y)}=\{(\pi/2\delta l_x)^2+(\pi/2\delta l_y)^2\}/(2M)=355.949$  in Eq. (37), irrespective to the value of  $v$ . Unperturbed energies are indicated by vertical lines on the  $z$  axis. The strip between two broken lines in (a) is a prediction of Eq. (51) with  $\alpha=1$ , on which the signature of wave chaos appears.

along with a restricted basis up to

$$E_{N(\Omega)} \approx (2M\Omega)^{-1}. \quad (47)$$

It is crucial that the zero-range approximation is justified as long as  $z \ll E_{N(\Omega)}$ , even if  $|V|$  is sufficiently large. The mixing among unperturbed eigenstates is limited to a small number of states even if  $v$  (or  $V$ ) is sufficiently large. Note also that the matrix  $\mathbf{V}$  has a bandlike structure, the width of which is independent of  $V$ , but is essentially determined by  $\Omega$ .

We can now describe the low-energy spectra of the billiards with a finite-size scatterer inside within the framework in Sec. II. It is realized from Eq. (42) that, as long as  $z \ll E_{N(\Omega)}$ , the eigenvalues in case of finite-size scatterer can be calculated by Eq. (18) with

$$\bar{v}_\theta^{-1} \approx v(\Omega)^{-1} + \alpha \ln(E_{N(\Omega)} - z) \approx v(\Omega)^{-1} + \alpha \ln E_{N(\Omega)}. \quad (48)$$

The meaning of the renormalized coupling constant  $\bar{v}_\theta$  becomes clear; A quantum billiard with a pointlike scatterer with strength  $\bar{v}_\theta$  can be obtained by taking the limit  $\Omega \rightarrow 0$  along with the limit

$$v(\Omega) = \frac{1}{\bar{v}_\theta^{-1} + \alpha \ln(2M\Omega)} \rightarrow -0, \quad (49)$$

or equivalently, with the limit

$$V = \frac{1}{\bar{v}_\theta^{-1}\Omega + \alpha\Omega \ln(2M\Omega)} \rightarrow -\infty. \quad (50)$$

Any two sets of  $(V, \Omega)$ , say  $(V_1, \Omega_1)$  and  $(V_2, \Omega_2)$ , which satisfy Eq. (50) with fixed  $\bar{v}_\theta$  describe the same low-energy dynamics as long as  $z \ll E_{N(\Omega)}$ , where  $\Omega = \max\{\Omega_1, \Omega_2\}$ . The logarithmic term in the denominator of Eq. (50) expresses the reason why we cannot define a pointlike scatterer in terms of a Dirac's  $\delta$  function in two dimension; the limit of  $\Omega \rightarrow 0$ , along with keeping  $V\Omega$  constant, induces a potential which is too strong to define a quantum mechanical Hamiltonian for a pointlike scatterer. It is noteworthy that in the small-size limit, the strength of the scatterer is always negative in the sense that  $V \rightarrow -\infty$  as  $\Omega \rightarrow 0$ . This is consistent with the fact that a single eigenstate with an eigenvalue smaller than  $E_1$  exists for any  $\bar{v}_\theta$ . We emphasize that this is not due to a specific formulation discussed here, but is required from the self-adjointness of the Hamiltonian. It should be noted, however, that as long as the obstacle has a substantial size, we can deduce all the low-energy physics from the present formulation by identifying  $v(\Omega)$  with  $\bar{v}_\theta$  through Eq. (48), even in the case of positive  $V$ .

Inserting Eq. (48) into Eq. (29), we obtain the condition for the appearance of the wave-chaotic energy spectrum,

$$\left| v(\Omega)^{-1} - \alpha \ln \frac{z}{E_{N(\Omega)} - z} \right| \leq \Delta \approx \alpha. \quad (51)$$

Keeping Eq. (23) in mind, we can rewrite Eq. (51) as

$$\left| \left( \frac{\langle \langle \mathbf{V} \rangle \rangle_{nn}}{\rho_{\text{av}}^{-1}} \right)^{-1} - \ln \frac{z}{E_{N(\Omega)} - z} \right| \leq 1. \quad (52)$$

Because the logarithmic function in Eq. (51) is negative for  $z < E_{N(\Omega)}/2$ , we obtain an interesting spectral property for lowest eigenstates: the wave chaos is most visible when the potential is attractive. As the energy increases up to  $z \approx E_{N(\Omega)}/2$ , the wave-chaotic region is expected to shift to  $|v(\Omega)^{-1}| \rightarrow 0$  according to Eq. (51). However, the zero-range approximation tends to lose its validity at high energy, particularly in attractive cases, as shown later in numerical calculations.

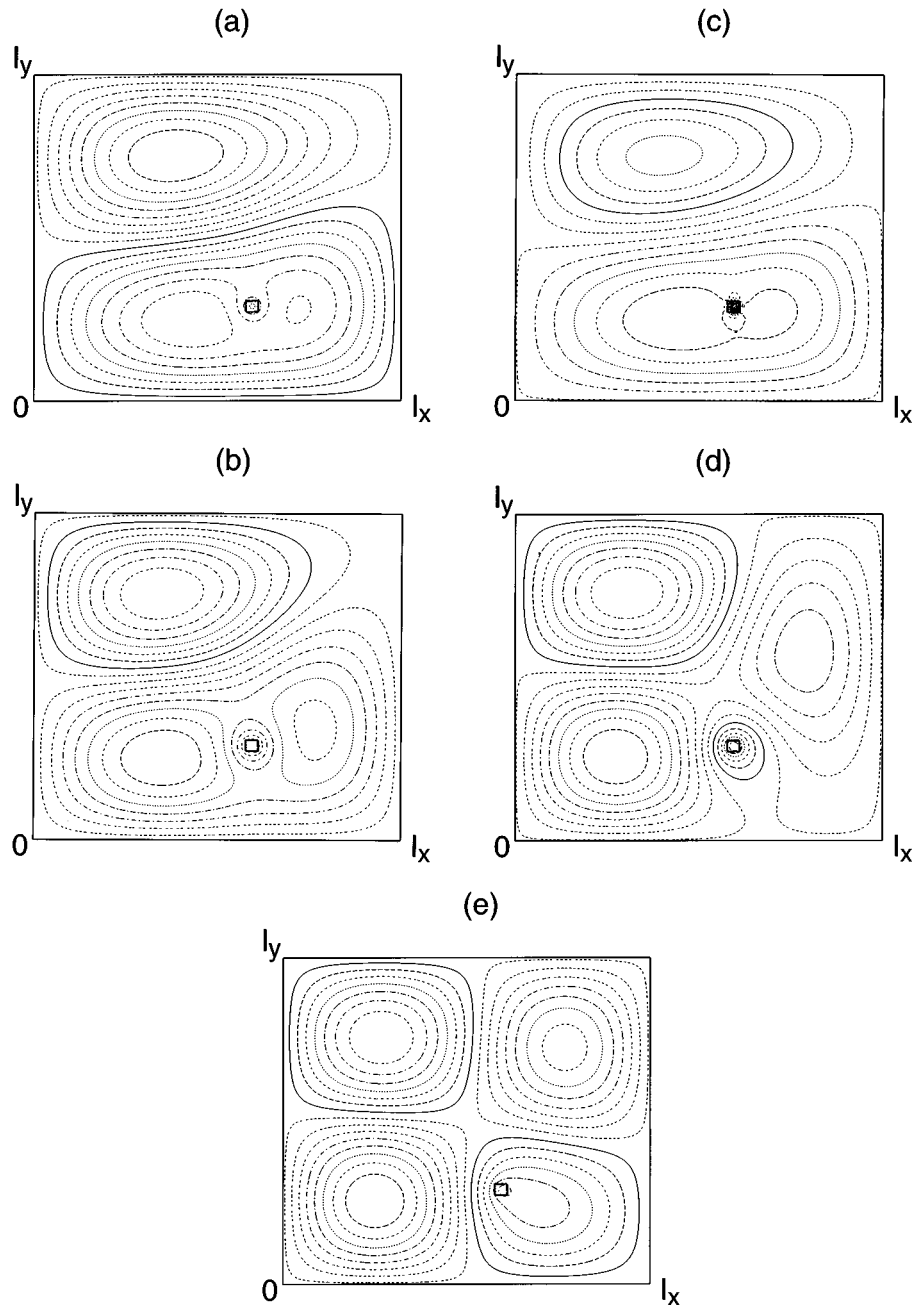


FIG. 2. The contour plot of the wave function for the eigenstates indicated by (a)–(e) in Fig. 1 is shown in (a)–(e), respectively. The value of  $(z, v^{-1})$  for the circles (a)–(e) is  $(4.54, 5.0)$ ,  $(4.93, 0.1)$ ,  $(4.43, -0.3)$ ,  $(5.63, -4.0)$ , and  $(6.13, -10.0)$ , respectively. The location of the scatterer is indicated by a rectangle in the billiard.

The previous numerical observations of Sinai’s billiard give supplementary evidence of the above finding. In Ref. [26], Berry exhibited the energy-level diagram of Sinai’s billiard as a function of the radius of a circular obstacle in the billiard. This reveals that the integrability is restored in the low-energy region as the radius decreases. This can be easily understood in the present scope. When the potential is repulsive, the wave chaos never appears even at low energy even if the repulsion is sufficiently strong. In spite of the infinite height of the potential in Sinai’s billiard, the limit of the radius being zero can be taken without any difficulty because only “desymmetrized states” are considered in Ref. [26].

In order to confirm the validity of Eq. (51), we examine the quantum spectra of a rectangular billiard with a small

rectangular scatterer inside, which is analogous to the system discussed in Ref. [8]. The unperturbed eigenvalues and the corresponding normalized eigenfunctions of the empty billiard are given by

$$E_{mn} = \frac{1}{2M} \left\{ \left( \frac{m\pi}{l_x} \right)^2 + \left( \frac{n\pi}{l_y} \right)^2 \right\} \quad (53)$$

and

$$\varphi_{mn}(x, y) = \left( \frac{4}{l_x l_y} \right)^{1/2} \sin \frac{m\pi x}{l_x} \sin \frac{n\pi y}{l_y}, \quad (54)$$

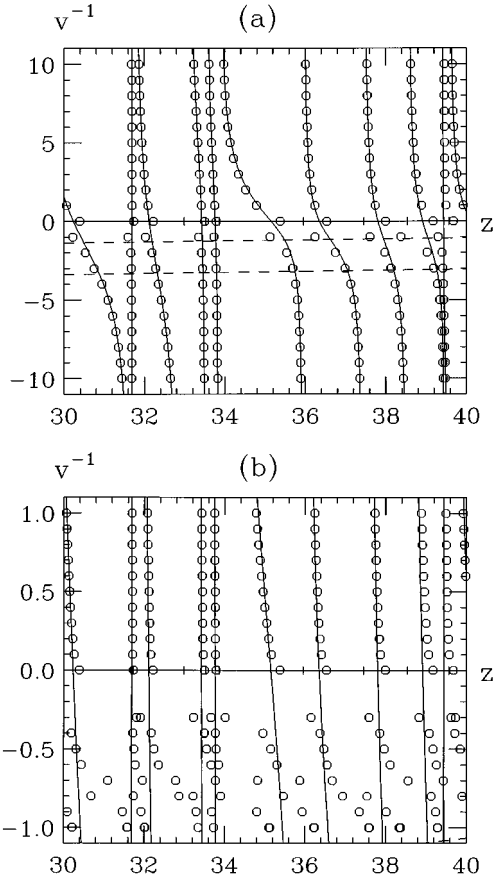


FIG. 3. The eigenvalues around  $z \approx 0.10E_{N(\delta l_x, \delta l_y)}$ . The indications are the same as in Fig. 1.

with  $m$  and  $n = 1, 2, 3, \dots$ , respectively. The side lengths of the (outer) rectangle are denoted by  $l_x$  and  $l_y$ . Suppose that a rectangular scatterer is placed inside the outer rectangle such that the sides of the inner and outer rectangles are parallel to each other. We denote the side lengths and the position of the center of the scatterer by  $\delta l_x$ ,  $\delta l_y$  and  $(x_0, y_0)$ ,

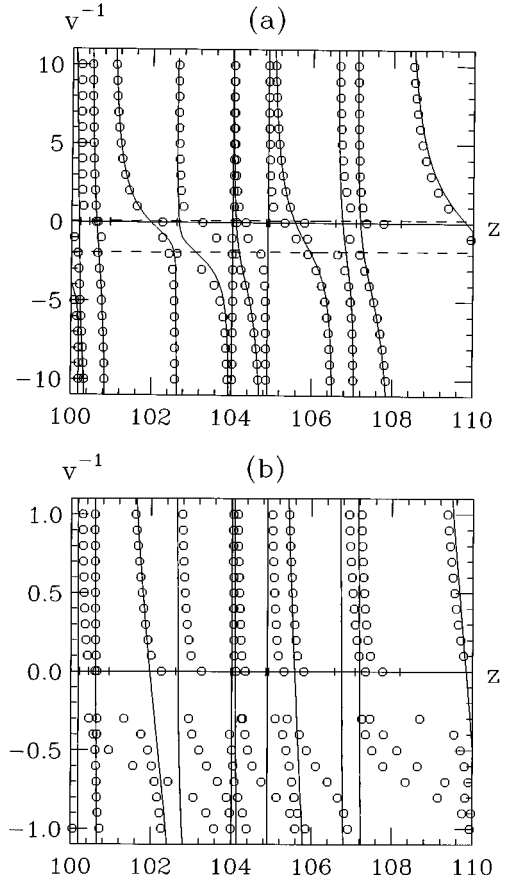


FIG. 4. The eigenvalues around  $z \approx 0.30E_{N(\delta l_x, \delta l_y)}$ . The indications are the same as in Fig. 1.

respectively. The matrix elements of the potential of Eq. (44) are given by

$$(\mathbf{V})_{m_1, n_1; m_2, n_2} = V u_{m_1, m_2}(l_x, \delta l_x, x_0) u_{n_1, n_2}(l_y, \delta l_y, y_0), \quad (55)$$

where

$$u_{m,n}(l, \delta l, x_0) = \begin{cases} \frac{2}{\pi} \left\{ \frac{1}{m-n} \cos \frac{(m-n)\pi x_0}{l} \sin \frac{(m-n)\pi \delta l}{2l} \right. \\ \left. - \frac{1}{m+n} \cos \frac{(m+n)\pi x_0}{l} \sin \frac{(m+n)\pi \delta l}{2l} \right\}, & m \neq n \\ \frac{\delta l}{l} - \frac{1}{n\pi} \cos \frac{2n\pi x_0}{l} \sin \frac{n\pi \delta l}{l}, & m = n. \end{cases} \quad (56)$$

In the actual numerical calculations, we set  $M = 2\pi$ ,  $l_x = \pi/3 = 1.04719$ , and  $l_y = 3/\pi = 0.954929$ , which leads to  $\rho_{av} = 1$  and  $\alpha \approx 1$ . We also assume  $\delta l_x = 3.53830 \times 10^{-2}$ ,  $\delta l_y = 3.14023 \times 10^{-2}$ , and  $x_0 = (x_0, y_0) = (0.622482, 0.275835)$ . In this choice, the area of the scatterer,  $\Omega$ , is 1/900 of the outer rectangle.

Figure 1(a) shows the several lowest eigenvalues of this system for various values of the inverse physical strength

$v^{-1}$ . The circles indicate the exact eigenvalues obtained by diagonalizing the Hamiltonian matrix along with Eq. (55). The strength of the scatterer  $V$  is determined by Eq. (46):  $V = v/\Omega$ . That is, a circle at  $(z, v^{-1})$  in Fig. 1(a) represents an eigenstate with eigenvalue  $z$  in case of potential height (depth)  $V = v/\Omega = 900/v^{-1}$  on the inner rectangular scatterer. The value of  $v^{-1}$  ranges from  $-10$  to  $10$  at intervals of  $1$ . We take  $v = 1000$  ( $V = 900000$ ) in the numerical calculation

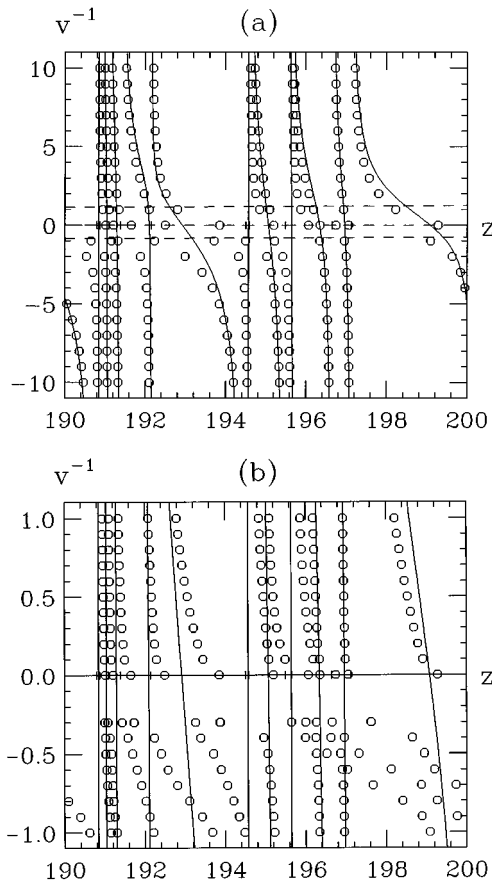


FIG. 5. The eigenvalues around  $z \approx 0.55E_{N(\delta l_x, \delta l_y)}$ . The indications are the same as in Fig. 1.

for  $v^{-1} = 0$ . The solid curves are the eigenvalues obtained by the approximation in terms of a Dirac's  $\delta$  function potential:  $V(\vec{x}) = v\delta(\vec{x} - \vec{x}_0)$ . As seen from Eq. (36), these curves are nothing but  $\tilde{G}(z)$  in Eq. (37). Following Eq. (47), we truncate the unperturbed basis at  $E_{N(\delta l_x, \delta l_y)} = \{(\pi/2\delta l_x)^2 + (\pi/2\delta l_y)^2\}/(2M) = 355.949$  in Eq. (37), irrespective of the value of  $v$ . This corresponds to making a truncation at the momenta  $k_x \approx \pi/(2\delta l_x)$  and  $k_y \approx \pi/(2\delta l_y)$ . From Fig. 1(a), we observe that the approximation of a zero-range potential with a suitably truncated basis is quite satisfactory, even if the potential is strong repulsion. Since we have  $v \approx \langle (\mathbf{V})_{m,n;m,n} \rangle / \rho_{av}^{-1}$  with  $\alpha \approx 1$ , the case of  $v = 1000$  ( $V = 900\,000$ ) indeed corresponds to a strong repulsion in the sense that the diagonal matrix elements of  $\mathbf{V}$  are far larger than the mean level spacing  $\rho_{av}^{-1}$  as well as the maximal unperturbed energy  $E_{N(\delta l_x, \delta l_y)}$  in the zero-range approximation. In case of a strong attractive potential, there is a considerable discrepancy between the exact and approximated eigenvalues. Figure 1(b) shows the eigenvalues for large  $|v|$ . When the scatterer is attractive, there exist, in general, several eigenstates with negative eigenvalues in case of finite-size scatterer; for example, three eigenstates with eigenvalues  $-1098$ ,  $-261$ , and  $-151$  for  $v^{-1} = -0.5$  ( $V = -1800$ ), and four eigenstates with eigenvalues  $-2182$ ,  $-1131$ ,  $-944$ , and  $-12$  for  $v^{-1} = -0.3$  ( $V = -3000$ ). (These values, particularly for shallow eigenstates, are not fully convergent despite a huge matrix diago-

nalization with 12 000 unperturbed states.) The eigenvalue of negative eigenstates is sensitive to the value of  $V$ . This causes a rapid change of the lowest positive eigenvalues as the potential strength varies. On the other hand, there is at most one negative eigenstate in the zero-range approximation, as seen from Eq. (36). Accordingly, the lowest positive eigenstates gradually change along the solid curves in Fig. 1(b). In particular, they are continuous even at  $v^{-1} = 0$ .

We emphasize that, since the summation in Eq. (37) diverges as  $N \rightarrow \infty$ , the appropriate truncation by Eq. (47) of the unperturbed basis is crucial for the success (except for the strong attraction) of the zero-range approximation.

As shown in Fig. 1(a), the inflection points of the solid curves in the low-energy region appear in a weakly attractive region. The prediction of Eq. (51), shown by a strip between two broken lines in Fig. 1(a), reproduces the position of the inflection points. Notice that, since the strip crosses the  $z$  axis around  $z \approx E_{N(\delta l_x, \delta l_y)}/2$  [see Eq. (51)], the inflection points appear on the attractive side at low energy,  $z \lesssim E_{N(\delta l_x, \delta l_y)}/2$ . In Fig. 2, we show the contour plot of the exact eigenfunction for several eigenstates obtained by diagonalizing the Hamiltonian matrix with the potential, Eq. (55). It can be seen that the mixture of the unperturbed eigenfunctions indeed occurs around the inflections points, while the wave function does not differ substantially from one of the unperturbed eigenfunctions in the region far from the inflection points. This indicates that, contrary to our naive intuition, the effects of the small scatterer in lowest eigenstates are most prominent in the weakly attractive case. We stress that, even if  $|v|$  is sufficiently large, the effects of high momentum components are visible mainly in the vicinity of the scatterer. The global behavior of eigenfunctions gradually changes as the potential strength varies.

Figures 3–5 show the eigenvalues in three cases:  $z \approx 0.10E_{N(\delta l_x, \delta l_y)}$  in Fig. 3,  $z \approx 0.30E_{N(\delta l_x, \delta l_y)}$  in Fig. 4, and  $z \approx 0.55E_{N(\delta l_x, \delta l_y)}$  in Fig. 5, respectively. It is observed that the accuracy of the zero-range approximation depends on the sign of the potential. For attractive cases, the zero-range approximation fails at somewhat low energy, as pointed out above. There is a considerable discrepancy even for  $v = -1$  ( $V = -900$ ) at  $z \approx 0.10E_{N(\delta l_x, \delta l_y)}$ . On the other hand, for repulsive cases, the approximated eigenvalues are in fairly good agreement with the exact eigenvalues up to  $z \approx 0.30E_{N(\delta l_x, \delta l_y)}$ . As the energy increases further, the zero-range approximation starts to fail except for in case of a very weak potential. It is easily recognized that the spectral properties of the exact eigenstates at high energy are subject to the geometry of the scatterer, since a quantum particle moving in the billiard tends to “see” the shape of the scatterer as the energy increases.

Finally, we make a comment on the size dependence of the scatterer. It is obvious that, as the size of scatterer shrinks, the zero-range approximation goes well even at higher energy. For a fixed energy in  $z \ll E_{N(\Omega)}$ , the effective strength  $v(\Omega)^{-1}$ , which satisfies the condition Eq. (51), approaches minus infinity as  $E_{N(\Omega)}$  becomes large. Thus we can expect that the wave-chaotic spectrum is observed with smaller value for  $|v|$  as the scatterer shrinks.

## VI. CONCLUSION

We have examined quantum spectra in two-dimensional billiards with a small-size scatterer inside. First, we clarified the spectral properties of pseudointegrable billiards with a pointlike scatterer from a general point of view. The strength of a pointlike scatterer is specified by a renormalized coupling constant  $\bar{v}_\theta$ , formally defined within the formulation based on functional analysis. Although the coupling constant does not have a direct relation to physical observables, it can be related to the physical coupling constant  $v$  defined as a strength of a Dirac's  $\delta$  function potential together with a truncated basis. In two-dimensional billiard problems, the zero-range interaction cannot be rigorously described in terms of a Dirac's  $\delta$  function. Nevertheless,  $v$  can be related to  $\bar{v}_\theta$  as long as the unperturbed basis is truncated at a finite number. From a physical perspective, the truncation of the

basis is a consequence of finiteness of the size of the scatterer, as the uncertainty principle implies. Applying the findings in pseudointegrable billiards to the cases of a small but finite-size scatterer, we have shown that the signature of wave chaos in lowest eigenstates are observed most prominently when the scatterer is weakly attractive. The numerical experiments of a rectangular billiard with a small rectangular scatterer inside corroborate these arguments.

## ACKNOWLEDGMENTS

One of the authors (T.S.) acknowledges the support of the Grant-in-Aid (No. 07740316) by the Ministry of Education, Science, Sports and Culture. Numerical calculations have been performed on the HITAC S-3800 supercomputer at the Computer Centre, the University of Tokyo.

- 
- [1] M. V. Berry and M. Tabor, Proc. R. Soc. London Ser. A **356**, 375 (1977).
  - [2] G. Casati, B. V. Chirikov, and I. Guarneri, Phys. Rev. Lett. **54**, 1350 (1985).
  - [3] M. L. Mehta, *Random Matrices and the Statistical Theory of Energy Levels* (Academic, New York, 1967), new revised and enlarged edition, 1990.
  - [4] O. Bohigas, *Random Matrix Theories and Chaotic Dynamics, Les Houches Summer School Proceedings Session 52*, edited by M.-J. Giannoni, A. Voros, and J. Zinn-Justin (North-Holland, Amsterdam, 1989).
  - [5] P. J. Richens and M. V. Berry, Physica D **2**, 495 (1981).
  - [6] K. Życzkowski, Acta Phys. Pol. B **23**, 245 (1992).
  - [7] A. N. Zemlyakov and A. B. Katok, Math. Notes **18**, 291 (1975).
  - [8] T. Cheon and T. D. Cohen, Phys. Rev. Lett. **62**, 2769 (1989).
  - [9] D. Biswas and S. R. Jain, Phys. Rev. A **42**, 3170 (1990).
  - [10] A. Shudo and Y. Shimizu, Phys. Rev. E **47**, 54 (1993).
  - [11] A. Shudo, Y. Shimizu, P. Šeba, J. Stein, H.-J. Stöckmann, and K. Życzkowski, Phys. Rev. E **49**, 3748 (1994).
  - [12] P. Šeba, Phys. Rev. Lett. **64**, 1855 (1990).
  - [13] T. Cheon, T. Mizusaki, T. Shigehara, and N. Yoshinaga, Phys. Rev. A **44**, R809 (1991).
  - [14] P. Šeba and K. Życzkowski, Phys. Rev. A **44**, 3457 (1991).
  - [15] T. Shigehara, N. Yoshinaga, T. Cheon, and T. Mizusaki, Phys. Rev. E **47**, R3822 (1993).
  - [16] T. Shigehara, Phys. Rev. E **50**, 4357 (1994).
  - [17] T. Cheon and T. Shigehara, Phys. Rev. E (to be published) (LANL e-print/hep-th/9512162).
  - [18] S. Albeverio, F. Gesztesy, R. Höegh-Krohn, and H. Holden, *Solvable Models in Quantum Mechanics* (Springer-Verlag, New York, 1988).
  - [19] M. Reed and B. Simon, *Methods of Modern Mathematical Physics, Vol. 2, Fourier Analysis, Self-adjointness* (Academic, New York, 1975).
  - [20] J. Zorbas, J. Math. Phys. **21**, 840 (1980).
  - [21] G. Flamand, in *Applications of Mathematics to Problems in Theoretical Physics*, edited by F. Lurcat (Gordon and Breach, New York, 1967).
  - [22] B. Simon, in *An Introduction to the Self-Adjointness and Spectral Analysis of Schrödinger Operators*, in *The Schrödinger Equation*, edited by W. Thirring and P. Urban (Springer-Verlag, Wien, 1977).
  - [23] J. von Neumann, *Mathematische Grundlagen der Quantenmechanik* (Springer-Verlag, Berlin, 1932) [English edition: *Mathematical Foundations of Quantum Mechanics* (Princeton University Press, Princeton, NJ, 1955)].
  - [24] R. L. Weaver and D. Sornette, Phys. Rev. E **52**, 3341 (1995).
  - [25] R. Jackiw, *Diverse Topics in Theoretical and Mathematical Physics* (World Scientific, Singapore, 1995).
  - [26] M. V. Berry, Ann. Phys. (N.Y.) **131**, 163 (1981).